Multiphoton Excited Conductance Spectroscopy. 1. Application of the Born Model to Femtosecond Laser Excited Multiphoton Ionization of Nonpolar Liquids

Jesse S. Greever, Joseph B M. Turner, and John F. Kauffman*

Department of Chemistry, University of Missouri, Columbia, Missouri 65211-7600

Received: February 22, 2001; In Final Form: July 12, 2001

A technique for determining the ionization potentials of pure liquid samples using visible wavelength femtosecond pulses is described. Exploiting a multiphoton ionization mechanism, we present values for the liquid-phase ionization potentials and compare them with estimated values calculated from gas phase ionization potentials. Estimates rely upon theoretical calculations of two values. First, the polarization energy of the solvent in the presence of a charged solute is calculated using the Born continuum solvation (BCS) model. Second, the conduction band of the liquid sample is calculated using the Springett−Jortner−Cohen (SJC) model, which corresponds to the stabilization energy of the free electron in the dielectric medium. Polarization energies are calculated with two different estimates of cavity radii, and comparisons are made to determine the adequacy of each set of radii. The striking agreement between the experimental results and theoretical predictions supports the viability of this technique as a straightforward method for determining liquid-phase ionization potentials using visible wavelength photons. It also supports the BCS model as an applicable method for calculating solvent polarization energies suitable for femtosecond photoionization.

Introduction

Ionization potentials of gas phase species are typically determined by photoelectron spectroscopy. Following photoionization with a VUV source or multiphoton ionization with a UV source, the excess kinetic energy of the electron is measured and subtracted from the excitation energy to give the ionization potential of the molecule under study. However, this method cannot be used in the liquid phase, because the kinetic energy of the ejected electron is quickly thermalized, and liquid-phase ionization potentials must be determined from VUV photoconductivity spectra.[1,2] Casanovas et al. have measured the ionization potentials of several neat liquids by plotting the conductivity values vs the excitation photon energy and imposing a conductivity threshold associated with free electron generation.[1,2] Faidas and Christophorou have determined solute ionization potentials of some organic aromatic chromophores such as azulene, pyrene, and fluoranthene by measuring two-photon to three-photon ionization photocurrents in dielectric liquids.[3−13] They arrive at ionization thresholds by imposing a condition on the excitation power dependence of the conductance profile in the spectral region that corresponds to a transition from two to three photons. However, in many cases, the results are complicated by resonance enhancement in the spectral region of interest, causing a broadening of the transition region and uncertainty in the ionization threshold.[11,12]

In addition to studies of ionization thresholds, numerous experimental studies have been reported that utilized liquid-phase multiphoton ionization for analytical and fundamental studies of solutes in condensed phases. Ogawa and co-workers have utilized multiphoton ionization of liquid samples for the quantitative analysis of aromatic samples in solution.[14−22] Kane et al. have utilized multiphoton ionization to study ion-induced nucleation in supersaturated vapors.[23] Femtosecond multiphoton ionization has enabled many researchers to study solvation dynamics of electrons in the solution phase,[24−27] and most of these studies focus on dynamics of hydrated electron solvation.[26,27] These recent studies have demonstrated the importance of multiphoton ionization in studies of charged species (primarily electrons) in condensed phases.

In this paper, we will show that the ionization potentials of low dielectric constant liquids can be determined from femtosecond multiphoton excited conductance spectra (fs-MPECS) using a tunable visible optical parametric amplifier. When the combined energy of the multiple photons exceeds the ionization potential, ionization occurs. The rate of generation of ions through the process of multiphoton ionization (MPI) is governed by eq 1.[28] The differential is the rate of production of the ionic

$$\frac{\mathrm{d}[\mathrm{M}^+]}{\mathrm{d}t} = \delta_n(\lambda) I^n(\lambda)[\mathrm{M}] \qquad (1)$$

species from the neutral species, M; $\delta_n(\lambda)$ is the excitation cross section, which reflects the wavelength-dependent probability of the molecule absorbing n photons simultaneously; the $I(\lambda)$ factor is the intensity of the light at wavelength λ, given as photon flux (photons $\mathrm{cm}^{-2}\ \mathrm{s}^{-1}$). The excitation cross section typically decreases as n increases and, in the case of processes involving more than three photons, can be lower than 10^{-100} [cm^{2n} (s^{n-1}·$\mathrm{photons}^{1-n}$)].[28] Therefore, the necessity for a comparably large intensity factor becomes evident. In the case of a three-photon process, I must be approximately 10^{28} photons $\mathrm{cm}^{-2}\ \mathrm{s}^{-1}$. Femtosecond pulses are capable of providing the photon flux required for multiphoton ionization.

On the basis of eq 1, a comparison of four- and five-photon ionization processes with the same photon flux should yield substantially different ion yields. For photon fluxes typical of our experiments ($I \sim 10^{30}$ photons $\mathrm{cm}^{-2}\ \mathrm{s}^{-1}$) and in the absence of resonant enhancements, the product of $\delta_n(\lambda)$ and $I^n(\lambda)$ is expected to be greater for a four-photon process than for a five-

* To whom correspondence should be addressed. E-mail: kauffmanj@missouri.edu.

10.1021/jp010692t CCC: $20.00
Published on Web 08/29/2001

photon process. By scanning through a range of wavelengths, the photon energy dependence of the ion yield can be observed for a given liquid sample, which allows for determination of the transition point that corresponds to the transition from *n*-photon excitation to $(n + 1)$-photon excitation. Additionally, the dependence of the ion yield on photon flux will differ in these two cases, because an *n*-photon process depends on the *n*th power of the intensity.

In this paper we investigate the applicability of fs-MPECS for determination of the ionization potentials of nonpolar liquid samples. Experimentally determined liquid-phase ionization potentials are compared against predicted values calculated from known gas-phase ionization potentials, ion solvation energies calculated from the Born continuum solvation (BCS) model for ion solvation, and solvent conduction band levels calculated with the Springett−Jortner−Cohen (SJC) model.[29] The remarkable agreement between experiment and theory validates our analysis and demonstrates that multiphoton ionization can be treated as a perturbative process under the conditions encountered in this study.

Experimental Section

The femtosecond laser source used for these experiments is a Clark-MXR CPA-2000 chirped pulse amplified Ti:sapphire laser. The system produces 800 mW of 775 nm light at 1000 Hz repetition rate. The typical pulse width is 120−150 fs (fwhm), as measured by interferometric autocorrelation. The 775 nm light is directed into an optical parametric amplifier (Clark-MXR Vis-OPA), to generate femtosecond laser pulses from 450−700 nm and an average power of approximately 3 mW at the sample. (Internal OPA optics include a frequency doubling crystal to generate the 388 nm OPA pump beam and a white light generator to seed the OPA.) The spectral bandwidth of the output of the OPA is approximately ±2.5 nm, corresponding to approximately ±0.015 eV energy bandwidth in the blue range of the OPA (450 nm) and ±0.0074 eV energy bandwidth in the red range of the OPA (650 nm).

The experimental setup for fs-MPECS measurements is shown in Figure 1. A small percentage of the beam (∼4%) is reflected by a quartz window and monitored by a photodiode (PD), which is used to determine the relative pulse intensity. The transmitted beam is collimated using a dual lens telescoping assembly (TA) and directed through a circular variable neutral density filter (FW). A computer-controlled stepper motor rotates the filter wheel through the 10% transmission to 100% transmission range. Though the laser pulse diameter was small and carefully controlled at the filter position, the circular variable neutral density filter may have caused slight heterogeneities in the transverse intensity profile. However, these heterogeneities are consistent in all experiments. A polarizer (POL) filters out any residual pump and second harmonic from the CPA-2000, which is cross-polarized with the signal from the OPA.

The filtered visible pulses are focused with a 50 mm focal-length achromat (AL) into a standard 1 cm quartz cuvette. The achromat maintains a fixed spot size inside the sample of approximately 100 μm diameter at the beam waist. A pair of stainless steel electrodes is suspended in the sample (800 μm electrode spacing) and positioned such that the focus of the laser beam is between the two electrodes, and a high voltage is applied (500−1500 V). When a pulse of light is present between the electrodes with sufficient photon flux to ionize the sample, the ionized species conduct current between the electrodes. The current is amplified by a current-to-voltage converter (*I*/*V* converter),[15] and the ion signal is collected as the attenuation

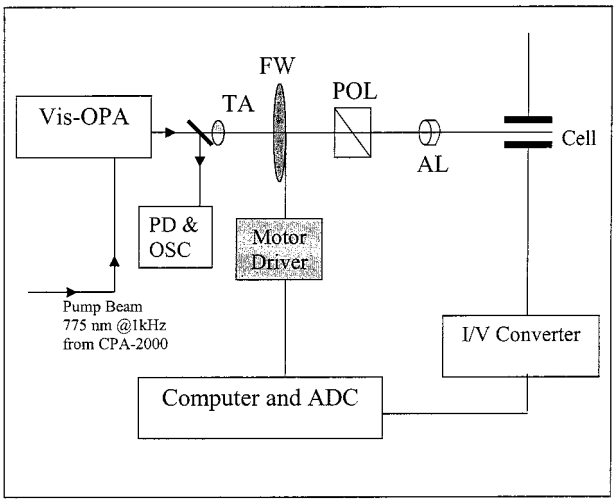

Figure 1. Instrumental setup for the fs-MPECS experiment. The OPA is pumped by the second harmonic of 775 nm. Tunable light from 450 to 650 nm is produced by the OPA and is directed toward a quartz window (QW), which sends approximately 4% of the beam into the photodiode (PD) with oscilloscope readout (OSC). The remaining beam is collimated in the telescoping lens assembly (TA) and sent through the variable density filter wheel (FW) driven by a computer interfaced stepper motor. The beam is then sent through a polarizer (POL) to eliminate any residual OPA pump and is then focused using an achromat lens (AL) into the sample cell. The current generated across the electrodes is detected and amplified, and the signal is digitized and compiled.

of the laser pulse is varied. The *I*/*V* converter has a calibrated gain of 2.02×10^8 V/A. Thus, an easily observable 10 mV signal pulse of 1 ms duration reflects the collection of approximately 10^6 charged particles. This crude estimate of detection level indicates that ∼1 amol of charged particles can be detected with our simple instrument. The intensity dependent photoionization current is measured incrementally at wavelengths between 450 and 650 nm (∼4 nm increments), and the ion signals at specific pulse intensities are tabulated and used to determine the ionization potential. The relative pulse intensity is determined according to the following expression:

$$I_{\text{eff}} = \frac{V_{\text{pd}} T}{R_{\text{d}}(\lambda)} \tag{2}$$

where I_{eff} is the effective relative pulse intensity, V_{pd} is the diagnostic voltage measured at the photodiode, T is the experimentally calibrated fractional transmittance of the ND filter wheel, and $R_{\text{d}}(\lambda)$ is the wavelength-dependent response of the photodiode. Since the relative pulse intensity (I_{eff}) is wavelength corrected and the spot size in the sample is fixed, it is possible to analyze each sample at a fixed relative intensity at various excitation wavelengths to obtain a wavelength-dependent fs-MPECS.

For the liquid samples, each of the solvents (*n*-pentane, cyclopentane, *n*-octane, triethylamine, carbon tetrachloride, benzene, toluene, and *p*-dioxane) was obtained in the highest purity available from Fischer Scientific and used as received. Each of the liquid samples was subjected to similar experimental conditions, with minor adjustments to optimize the measurement (i.e., adjustment of applied potential to compensate for low ion signal).

In performing the experiments, we have observed a phenomenon related to the important issue of sample heating. The primary mechanism of sample heating in this experiment is thermalization of the ionization energy following electron−

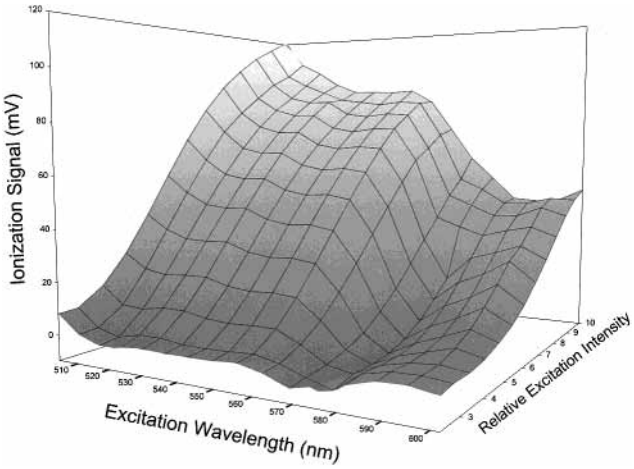

Figure 2. fs-MPECS excitation surface for *n*-pentane. The plot shows the dependence of the conductance signal on the excitation wavelength and the excitation power monitored by a photodiode. The data show a distinct drop in photocurrent between 560 and 570 nm.

cation recombination. In the absence of a dc field, the resulting localized heating takes place within the irradiated zone and leads to density fluctuations, and therefore substantial Rayleigh scattering of the excitation beam. However, the Rayleigh scattering is significantly reduced when the dc field is applied because electron−cation recombination is inhibited by field-induced charge separation. (This phenomenon is under further investigation.) This effect is easily observable by eye, and the scattering observed in the presence of the field is similar to scattering of a low power continuous wave (cw) laser beam. This indicates that the heat due to ionization is dissipated throughout the sample volume located between the electrodes and at the electrode surfaces. We use less than 5 mW of average laser power, and most of this power is transmitted through the sample. Because we are able to "quench" the recombination, localized sample heating in the irradiated zone is substantially reduced. At this time we do not have a quantitative measure of the local sample temperature in the irradiated zone. While sample heating may influence the measured current, this study is aimed at identifying and analyzing the sharp transitions in conductivity that are expected when the photon order changes as a result of changes in the excitation wavelength, not in the absolute conductivity levels. Local heating may affect the signal level, but it should not affect the position of the transition we seek, particularly because the transitions we observe are sharp.

Results

For each solvent, power dependent scans were taken at wavelength increments across the 500−650 nm range in order to form a conductance excitation surface. For example, the conductance surface of *n*-pentane spanning its four- and five-photon regions is shown in Figure 2. This surface shows a sharp transition at 568 nm. Not only does the magnitude of the conductance signal decrease on the long wavelength side of this transition, the shape of the power response changes as well. The signal transition corresponds to a transition from four- to five-photon ionization. The shape of the power dependence, which is shown in Figure 3, assumes a markedly different form on either side of the transition as expected. This is also indicative of a transition from a four- to five-photon process. It is worth mentioning that there is a significant saturation effect in each of the intensity dependence profiles. After a certain excitation intensity is achieved, the conductance no longer responds to increases in excitation intensity according to the exponential

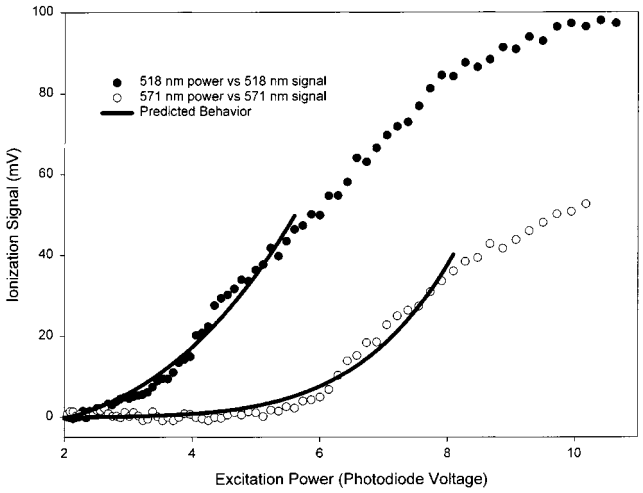

Figure 3. Conductance power dependence of *n*-pentane at two excitation wavelengths. The solid lines are curves that correspond to $y = ax^n$, where $n = 4$ for the 518 nm curve and $n = 5$ for the 571 nm curve. Both plots exhibit ion current saturation at higher effective excitation intensities (for approximate excitation intensity >5.5 for 518 nm and excitation intensity >8 for 571 nm).

power law (I^n) but tends to plateau. This saturation phenomenon is under further investigation, as to whether it is the result of a physical phenomenon or a limitation of photocurrent detection. There is a noticeable difference in the excitation intensity threshold for saturation, with the four-photon (518 nm) conductance saturating at much lower excitation intensity than the five-photon (571 nm) conductance.

Figure 4 presents fs-MPEC spectra of three liquids at constant excitation power. The plots reveal the transition from four- to five-photon ionization (4a and 4b) and from three- to four-photon ionization (4c). The response of the conductance signal with respect to the excitation energy behaves as expected, with a sharp decrease occurring in the range 550−570 nm for *n*-pentane and cyclopentane and 510−525 nm for toluene. To characterize a transition wavelength objectively, we fit the fs-MPECS data to a modified sigmoidal function given in eq 3.

$$f(\lambda) = y_0 + \frac{a}{[1 + e^{-(\lambda-\lambda_0)/b}]^c} + u(\lambda_0)[d(\lambda - \lambda_0)] + (1 - u(\lambda_0))[g(\lambda - \lambda_0)] \quad (3)$$

The first two terms comprise a common five-parameter sigmoidal function. The third and fourth terms are linear terms, which allow the data to be fitted to slightly sloping regions on either side of the transition point, rather than the standard sigmoidal function, which assumes flat regions (slope = 0) on either side of the transition. The fitting parameter of consequence is the λ_0 term, which is the central point of the sharp transition. The $u(\lambda_0)$ term is the unit step function centered on the transition wavelength, λ_0. Adding the unit step function to the sigmoid allows the additive linear functions on either side of the transition point to be fitted independently. This, in turn, results in a better estimate of λ_0 for all solvents. In physical terms, λ_0 is taken to be the transition between *n*-photon ionization on the short wavelength side and $(n + 1)$-photon ionization on the long wavelength side of the transition. At wavelengths greater than λ_0, $(n + 1)$ photons are required to exceed the ionization potential. Therefore, the ionization potential is taken to be the product of *n* and $h\nu$, which corresponds to the point at which *n* photons reaches the minimum energy of the ionization continuum.

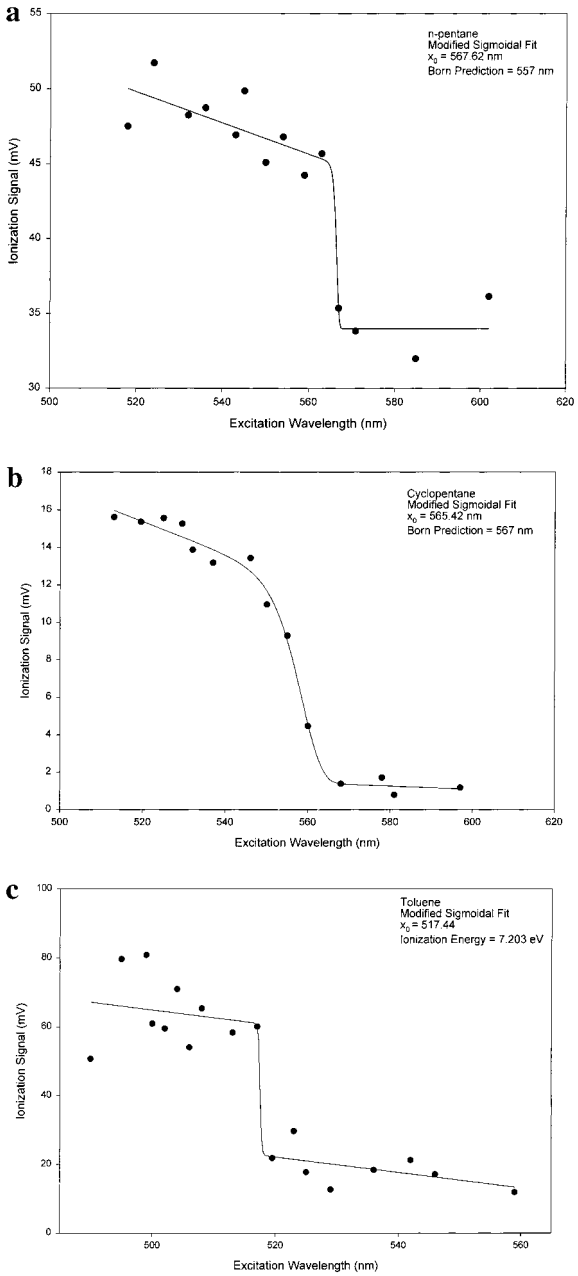

Figure 4. Photoionization excitation spectrum of (a) *n*-pentane, (b) cyclopentane, and (c) toluene fit to the eq 3. Wavelengths predicted on the basis of the BCS model of cation solvation and gas-phase ionization potentials are listed for each liquid.

The measured transition wavelengths (λ_0) for several solvents are compiled in Table 1. From these, experimental values for the liquid phase ionization potential have been calculated. These have been compared with the predicted values calculated from experimentally determined gas-phase ionization potentials (IP_g)[38] and terms that account for solvation of the cation and the electron produced by photoionization. Our experimental values for *n*-pentane and cyclopentane have also been compared to experimental values from the VUV measurements of Casanovas et al.[1] The expression for the predicted liquid-phase ionization potential (IP_l) is[30]

$$IP_l = IP_g + P_{pol} + V_0 \tag{4}$$

where P_{pol} is the polarization energy of the solvent around the cation, and V_0 is the conduction band energy of the solvent, which accounts for the solvation energy of the electron. The

TABLE 1: Experimental Data for fs-MPECS of Liquid Samples[a]

sample	λ_0 (nm)	*n* (photons)	exptl IP_l (eV)	lit. IP_l (eV)
TEA	642	3	5.808	
toluene	517	3	7.213	
benzene	498	3	7.488	
dioxane	488	3	7.641	
c-pentane	565	4	8.800	8.82[1]
n-octane	565	4	8.800	
n-pentane	568	4	8.754	8.86[1]
CCl_4	497	4	10.004	

[a] λ_0 corresponds to transition wavelength, *n* represents the number of photons required for ionization. TEA is triethylamine.

polarization energy for each solvent has been calculated using the BCS model for a charged particle in a dielectric continuum.[31] The BCS model assumes that a solvated charged particle can be treated as a point charge at the center of a spherical cavity that is present in a continuum solvent characterized by ϵ, the bulk dielectric constant. The expression for stabilization due to solvation is given in eq 5 and is also dependent upon the charge

$$P_{pol} = -\frac{1}{8\pi\epsilon_0}\left(1 - \frac{1}{\epsilon}\right)\left(\frac{q^2}{r}\right) \tag{5}$$

of the cation (q) and the spherical cavity radius (r). The polarization energy is quadratically dependent upon the charge of the cation (q); however, since the probability of reaching the second ionization potential in these experiments is negligible, the ionic charge (q) is assumed to be +1. We associate the spherical cavity radii with the size of the solvents and two different methods for calculating radii were used. The first set of radii was determined using the van der Waals *b* coefficient for each solvent.[35] The second set of solvent radii was determined using the method prescribed by Bondi for estimating van der Waals radii.[32] The polarization energies for the solvents were calculated using both radii, and are given in Table 2.

The conduction band energy (V_0) reflects the response of the solvent around the free electron produced in the photoionization process. Holroyd has shown that the experimental values of V_0 in molecular liquids are in agreement with theoretical predictions based on the Springett−Jortner−Cohen model.[33] This method breaks the energy contribution into a sum of two terms, as shown in eq 6: a potential energy term describing the polarization of the medium around the electron (U_{pol}) and an electron kinetic energy term (T).

$$V_0 = T + U_{pol} \tag{6}$$

The potential energy term accounts for the polarizability (α), density (ρ_0), and the Wigner−Seitz radius of the solvent molecule (r_s) according to the following expression:

$$U_{pol} = -\left(\frac{3\alpha e^2}{2r_s^4}\right)\left[\frac{8}{7} + \left(1 + \frac{8}{3}\pi\alpha\rho_0\right)^{-1}\right] \tag{7}$$

where r_s is derived from the bulk solvent density, given by

$$r_s^3 = \frac{3}{4\pi\rho_0} \tag{8}$$

The electron kinetic energy term is determined from the mass of the electron (m_e) and the wave vector (k_0) that describes the ground state of the system according to eq 9. The wave vector

TABLE 2: Comparison of Predicted Values (vdW IP_l, Bondi IP_l) Based on van der Waals Radii (vdW *r*) and Bondi Radii (Bondi *r*) and Experimentally Determined Values (Exptl IP_l)[a]

sample	IP_g (eV)	vdW *r* (Å)	vdW P_{pol}(eV)	Bondi *r* (Å)	Bondi P_{pol} (eV)	V_0 (eV)	exptl IP_l (eV)	vdW IP_l (eV)	% error vdW	Bondi IP_l (eV)	% error Bondi
TEA	7.53	2.63	−1.61	3.11	−1.36	−0.10	5.81	5.82	0.2	6.07	4.5
toluene	8.83	2.44	−1.71	2.87	−1.45	−0.20	7.21	6.92	−4.0	7.18	−0.4
benzene	9.24	2.25	−1.80	2.68	−1.51	−0.11	7.49	7.33	−2.1	7.62	1.7
dioxane	9.19	2.42	−1.63	3.01	−1.31	−0.27	7.64	7.29	−4.6	7.61	−0.4
c-pentane	10.33	2.27	−1.56	2.88	−1.23	0.11	8.80	8.88	0.9	9.21	4.7
n-octane	9.80	2.86	−1.23	3.28	−1.07	−0.09	8.80	8.48	−3.6	8.64	−1.8
n-pentane	10.28	2.44	−1.34	2.84	−1.16	0.04	8.75	8.98	2.6	9.16	4.7
CCl_4	11.47	2.39	−1.67	2.73	−1.46	−0.27	10.00	9.53	−4.7	9.74	−2.6

[a] Conductance band energies (V_0) calculated using SJC model. TEA is triethylamine.

$$T = \frac{\hbar^2 k_0^2}{2m_e} \tag{9}$$

term, k_0, is determined from the boundary conditions of the ground-state quasi-free electron pseudo-wave function and can be obtained from the following expression:

$$\tan[k_0(r_s - a)] = k_0 r_s \tag{10}$$

where *a* is the so-called electron molecule hard core radius that has been shown empirically to be related to the critical volume (V_{crit}) by $a = 0.303\ V_{crit}^{1/3}$ (where V_{crit} is in units of cm^3/mol and *a* is in angstroms). The V_0 term is relatively small compared to P_{pol} and in most cases is a small stabilization (negative value), with *n*-pentane and cyclopentane being the only exceptions. The conduction band energy generally tends to decrease as the size of alkanes increases, due to the dependence on the Wigner−Seitz radius, and therefore, the two smaller alkanes are the only two molecules with positive V_0.

In Table 2, theoretically predicted values of IP_l based on radii calculated from the van der Waals *b* coefficient and the Bondi method are compared against the experimentally determined values. The radii determined from the van der Waals *b* coefficients are smaller than those calculated by the Bondi method, and therefore give systematically lower values of P_{pol}. Therefore, the predicted liquid-phase ionization potentials calculated using the polarization energy based on the van der Waals (vdW P_{pol}) radii are systematically lower than those predicted on the basis of the Bondi method. An examination of the percent deviation from the experimentally determined values reveals that predictions based upon the use of the van der Waals *b* coefficient tend to underpredict the experimental values, and the predictions based upon the use of the Bondi method tend to overpredict the experimental values. However, the average percent error for the van der Waals predicted values (−1.9%) is slightly greater in absolute magnitude than the average percent error for the Bondi predicted values (1.3%). Figure 5 shows the experimentally determined values of IP_l plotted against the predicted values for IP_l determined from Bondi calculated radii. The excellent correlation between theory and experiment validates both the experimental method and the applicability of the Born model for solvation of ions in nonpolar liquids. Furthermore, the use of either the van der Waals *b* coefficient or radii estimated by the Bondi method lead to reasonable calculated values of P_{pol}.

Figure 6 illustrates a complication that arose when studying benzene. In most cases, the samples studied have wide electronic energy level spacing, reducing the probability of resonances with intermediate states. A two-photon resonance will increase the overall photoionization cross-section. In the case of benzene, the predicted transition from the three- to four-photon region

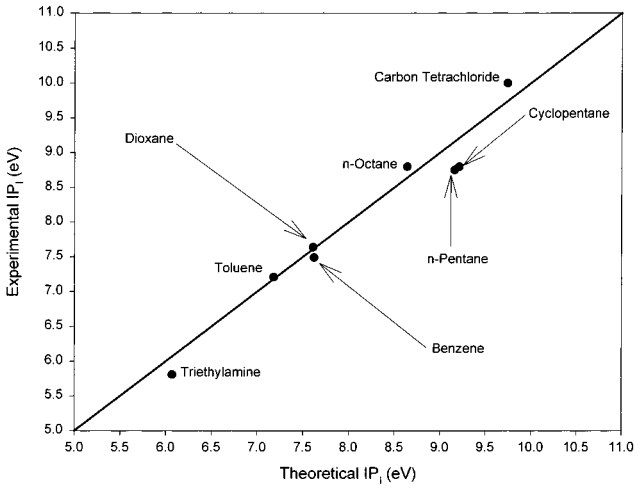

Figure 5. Comparison of experimentally determined IP_l values with predicted values. The bold line indicates an ideal correlation with predicted values using the Bondi radii.

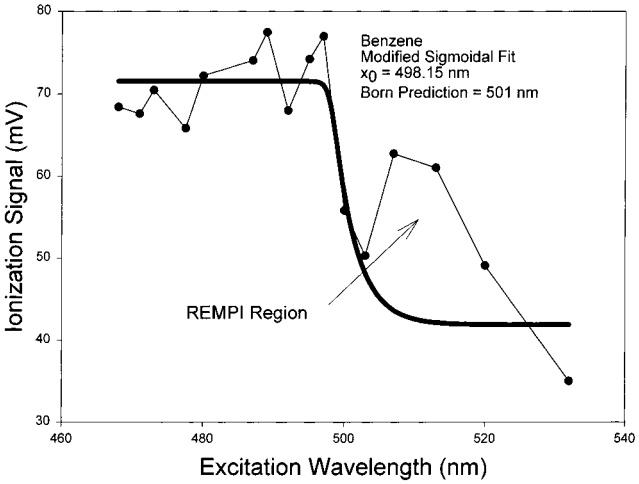

Figure 6. fs-MPECS of benzene, fit to eq 3. The predicted value of the three- to four-photon transition occurs at 501 nm (7.45 eV), while the spectrum shows a transition at 498 nm (7.49 eV). The labeled REMPI region is the area where enhancement of conductance occurs due to two-photon resonance with an excited state at approximately 254 nm, which increases the photoionization cross-section. When fitting the data, the two points affected by the REMPI enhancement were omitted.

occurs within approximately 10 nm of a two-photon resonance with an excited state at approximately 254 nm, which is labeled in Figure 6 as the REMPI (resonantly enhanced multiple photon ionization) region. It is evident from the spectrum that there is enhancement of the four-photon ionization resulting from a resonance with the electronic state at 254 nm,[34] which corresponds to a two-photon wavelength of 508 nm. Figure 6 shows

that the three- to four-photon ionization transition occurs near the REMPI region, and an increase in the four-photon signal is observed immediately above the transition.

Discussion

The excellent agreement of the experimental data with the theoretical predictions of the BCS model motivates a few important points. First, the BCS model accurately describes the energy difference between a solvated ion and a gas-phase ion (P_{pol}) in nondipolar solvents. This indicates that the simple point-charge form of the BCS model is sufficient for the calculation of P_{pol}, and use of a more complex form for the model,[31] which takes into account the charge distribution of the solvated ion, is not expected to be accompanied by a large improvement in the predicted value of the liquid phase ionization potential. Second, the validity of the BCS model for the ionization event indicates that the molecule being ionized senses the presence of the solvent throughout the ionization process. That is, in the case of nondipolar solvents the solvent dielectric constant characterizes the response of the solvent to a fast variation in the charge distribution of the species that is ionized. This observation is not unexpected in the case where the solvent polarization energy is dominated by the solvent electronic response. However, dipolar solvents may not exhibit the same agreement between experiment and theory, because solvent polarization due to orientational reorganization is a much slower process, and the BCS model does not explicitly recognize the temporal behavior of the solvent dielectric response. Of the molecules in this study, only two have permanent dipole moments, and of those, neither is larger than 0.9 D (triethylamine, $\mu = 0.9$ D; toluene, $\mu = 0.45$ D).[35] Examination of the data for toluene and triethylamine indicates that the dipolar contribution of the solvent is sufficiently small and causes a negligible error in the prediction of the experimental value.

Agreement with the BCS model also indicates that under the conditions of this study (maximum laser field for this study is ~0.06 V/Å), femtosecond multiphoton ionization is a perturbative phenomenon and precludes the possibility of field ionization.[36] Field ionization, while not an issue for XUV ionization experiments, is possible with femtosecond pulses that have fields on the order of 1 V/Å,[37] which are sufficient to alter the energy level structure of the molecule. At these fields, the electrostatic term in the molecular Hamiltonian cannot be treated perturbatively.[36] The result of this treatment is the appearance of significantly altered energy levels (dressed states) arising from strong coupling of unperturbed states. When field ionization occurs, a simple treatment of the cation solvation energy is not adequate, and an exact solution to the complete Hamiltonian is required to determine the energies of the dressed states, and therefore the dressed ionization threshold. The fact that the BCS model correctly predicts the observed ionization potentials indicates that we are indeed in the perturbative regime under our experimental conditions, a result that is not unexpected given the fact that we are nearly 2 orders of magnitude below the field ionization threshold.

The fs-MPECS technique is a high-resolution method for determination of liquid phase ionization potentials. Despite the bandwidth of the femtosecond laser system, which is approximately ±2.5 nm (±0.011 eV) at the center of the tuning range of the OPA (~532 nm), propagation of the uncertainty due to bandwidth for a four-photon ionization gives an overall uncertainty of ±0.022 eV. To achieve this resolution using a VUV source at the equivalent wavelength (133 nm), a source bandwidth of ±0.032 nm is required, whereas typical measurements report bandwidths in the range of ±1 nm.

In all but a few cases, the ionized species have very low symmetry, and therefore symmetry selection rules play a very small role in these experiments. The fact that the molecules are being excited directly into the ionization continuum via a nonresonant pathway (except for the case of benzene) also indicates that selection rules do not play a dominant role in these experiments, due to the effectively infinite density of states in the continuum and the high coupling between "allowed" and "forbidden" states.

Conclusions

The measurements described in this work demonstrate that the liquid-phase ionization potentials of pure liquids can be determined without the use of extremely high energy photons by using tunable femtosecond visible wavelength pulses. fs-MPECS measurements can be performed without the need for deep ultraviolet optics and high-energy photon sources. The experiments are straightforward, involving detection of a well-defined transition that can be easily fit to a modified sigmoidal function. The concentration of ions in the space between the electrodes is high enough that conductance measurements require very little signal manipulation. This method also provides a technique for preparing a transient high ion-density sample in low polarity liquids, which may be useful for the study of solvation dynamics around ionic species.

Acknowledgment. The laser system used for this investigation was purchased with funds provided in part by the National Science Foundation (CHE-9708896).

References and Notes

(1) Casanovas, J.; Grob, R.; Delacroix, D.; Guelfucci, J. P.; Blanc, D. *J. Chem. Phys.* **1981**, *75*, 4661.
(2) Casanovas, J.; Grob, R.; Sabattier, R.; Guelfucci, J. P.; Blanc, D. *Radiat. Phys. Chem.* **1980**, *15*, 293.
(3) Siomos, K.; Christophorou, L. G. *Chem. Phys. Lett.* **1980**, *72*, 43.
(4) Siomos, K.; Kourouklis, G.; Christophorou, L. G.; Carter, J. G. *Radiat. Phys. Chem.* **1980**, *15*, 313.
(5) Siomos, K.; Kourouklis, G.; Christophorou, L. G. *Chem. Phys. Lett.* **1981**, *80*, 504.
(6) Siomos, K.; Kourouklis, G.; Christophorou, L. G.; Carter, J. G. *Radiat. Phys. Chem.* **1981**, *17*, 185.
(7) Siomos, K.; Kourouklis, G.; Christophorou, L. G.; Carter, J. G. *Radiat. Phys. Chem.* **1981**, *17*, 75.
(8) Kourouklis, G. A.; Siomos, K.; Christophorou, L. G. *Chem. Phys. Lett.* **1982**, *88*, 572.
(9) Siomos, K.; Christophorou, L. G. *J. Electrost.* **1982**, *12*, 147.
(10) Faidas, H.; Christophorou, L. G. *J. Chem. Phys.* **1987**, *86*, 2505.
(11) Faidas, H.; Christophorou, L. G. *Radiat. Phys. Chem.* **1988**, *32*, 433.
(12) Faidas, H.; Christophorou, L. G. *J. Chem. Phys.* **1988**, *88*, 8010.
(13) Faidas, H.; Christophorou, L. G.; Datskos, P. G.; McCorkle, D. L. *J. Chem. Phys.* **1989**, *90*, 6619.
(14) Ogawa, T.; Kise, M.; Yasuda, T.; Kawazumi, H.; Yamada, S. *Anal. Chem.* **1992**, *64*, 1217.
(15) Yamada, S.; Ogawa, T. *Anal. Chim. Acta* **1986**, *183*, 251.
(16) Yamada, S.; Sato, N.; Kawazumi, H.; Ogawa, T. *Anal. Chem.* **1987**, *59*, 2719.
(17) Chen, H.; Inoue, T.; Ogawa, T. *Anal. Chem.* **1994**, *66*, 4150.
(18) Kawazumi, H.; Isoda, Y.; Ogawa, T. *J. Phys. Chem.* **1994**, *98*, 170.
(19) Nakashima, K.; Kise, M.; Ogawa, T.; Kawazumi, H.; Yamada, S. *Chem. Phys. Lett.* **1994**, *231*, 81.
(20) Ogawa, T.; Chen, H.; Inoue, T.; Nakashima, K. *Chem. Phys. Lett.* **1994**, *229*, 328.
(21) Ogawa, T.; Sato, M.; Tachibana, M.; Ideta, K.; Inoue, T.; Nakashima, K. *Anal. Chim. Acta* **1995**, *299*, 355.
(22) Ogawa, T.; Ogawa, T.; Nakashima, K. *J. Phys. Chem. A* **1998**, *102*, 10608.
(23) Kane, D.; Rusyniak, M.; Fisenko, S. P.; El-Shall, M. S. *J. Phys. Chem. A* **2000**, *104*, 4912.
(24) Long, F. H.; Lu, H.; Eisenthal, K. B. *J. Phys. Chem.* **1995**, *99*, 7436.

(25) Lu, H.; Long, F. H.; Eisenthal, K. B. *J. Opt. Soc. Am. B: Opt. Phys.* **1990**, *7*, 1511.

(26) Assel, M.; Laenen, R.; Laubereau, A. *J. Chem. Phys.* **1999**, *111*, 6869.

(27) Silva, C.; Walhout, P. K.; Yokoyama, K.; Barbara, P. F. *Phys. Rev. Lett.* **1998**, *80*, 1086.

(28) Shear, J. B. *Anal. Chem.* **1999**, *71*, 598A.

(29) Springett, B. E.; Jortner, J.; Cohen, M. H. *J. Chem. Phys.* **1968**, *48*, 2720.

(30) Holroyd, R. A.; Russell, R. L. *J. Phys. Chem.* **1974**, *78*, 2128.

(31) Qiu, D.; Shenkin, P. S.; Hollinger, F. P.; Still, W. C. *J. Phys. Chem. A* **1997**, *101*, 3005.

(32) Bondi, A. *J. Phys. Chem.* **1964**, *68*, 441.

(33) Holroyd, R. A.; Tames, S.; Kennedy, A. *J. Phys. Chem.* **1975**, *79*, 2857.

(34) Birks, J. B. *Photophysics of Aromatic Molecules*; John Wiley & Sons: London, 1970.

(35) Dean, J. A. *Lange's Handbook of Chemistry*; McGraw-Hill: New York, 1992.

(36) Craig, D. P.; Thirunamachandran, T. *Molecular Quantum Electrodynamics: An Introduction to Radiation−Molecule Interactions*; Dover Publications: New York, 1998.

(37) DeWitt, M. J.; Levis, R. J. *J. Chem. Phys.* **1999**, *110*, 11368.

(38) IP_g values obtained from references compiled in the NIST Chemistry Webbook, http://webbook.nist.gov/chemistry. The following references were listed in the database: Lloyd, D. R.; Bassett, P. J. *J. Chem. Soc. A* **1971**, 641. Meot-Ner, M.; Sieck, L. W.; Ausloos, P. *J. Am. Chem. Soc.* **1981**, *103*, 5342. Mathis, J. E.; Compton, R. N. *J. Chem. Phys.* **1996**, *104*, 8341. Lu, K. T.; Eiden, G. C.; Weisshaar, J. C. *J. Phys. Chem.* **1992**, *96*, 9742. Nemeth, G. I.; Selzle, H. L.; Schlag, E. W. *Chem. Phys. Lett.* **1993**, *215*, 151. Fraser-Monteiro, M. L.; Fraser-Monteiro, L.; Butler, J. J.; Baer, T.; Hass, J. R. *J. Phys. Chem.* **1982**, *86*, 739. Lias, S. G. *Lect. Notes Chem.* **1982**, *31*, 409.